

## Using stable isotopes and gas concentrations for independent constraints on microbial methane oxidation at Arctic Ocean temperatures

Christiane Uhlig \* Brice Loose

Graduate School of Oceanography, University of Rhode Island, Narragansett, Rhode Island

### Abstract

Microbial oxidation of methane in oxic water bodies is an important control on the amount of dissolved methane which is released from the ocean to the atmosphere. We explored the use of stable isotope methane spikes to quantify methane oxidation rates in Arctic seawater samples. A Picarro G2201-*i* cavity ring-down spectrometer was used to determine methane concentration and isotope ratios from headspace samples in foil incubators. The methane mass balance and the change in stable isotope ratios served as independent constraints on methane oxidation. For a fractionation factor of 1.025 oxidation rate constants determined with both methods agreed within 20% for small changes in isotope ratio (e.g., 10‰). For large changes in isotope ratio (e.g., 90‰), which was outside the calibration range, methods diverged. Rate constants down to 0.01 d<sup>-1</sup> could be resolved with high statistical support. Stable isotope infrared spectroscopy to determine methane oxidation in foil incubators (ISMOFI) was successfully tested on under ice seawater from Utqiagvik, Alaska, by repeated sampling from each incubation vessel. Depending on the amount of isotope spike added, we determined oxidation rates of 0.15 ± 0.02 nmol L<sup>-1</sup> d<sup>-1</sup> at in situ methane concentration and a maximal oxidation potential of 271 ± 41 nmol L<sup>-1</sup> d<sup>-1</sup>. The ISMOFI method permits variable incubation durations from days to months in a single incubator. The method is transportable and applicable in a variety of field or seagoing laboratory environments, and it avoids the use of hazardous substances such as radioisotopes and toxic chemicals.

Besides carbon dioxide and water vapor, methane (CH<sub>4</sub>) is one of the most important greenhouse gases contributing to global warming (IPCC 2013). In the ocean, the two major sources of methane are the production by microbes in anoxic sediments (e.g., Whiticar 1999; Reeburgh 2007; Formolo 2010) and the release from geological storages (summarized by Kvenvolden and Rogers 2005; Saunio et al. 2016). Most of this methane is subsequently oxidized inside the sediment by anaerobic and aerobic oxidation (Barnes and

Goldberg 1976; Reeburgh 1976; Knittel and Boetius 2009; Boetius and Wenzhöfer 2013). The fraction of methane, which is actually being released to the water column, is subject to further oxidation by aerobic methanotrophic bacteria (Hanson and Hanson 1996; Murrell 2010). As a result of these microbial processes, oceanic methane concentrations are frequently found at low nanomolar levels, leaving only a small fraction of the source methane to exchange with the atmosphere (Reeburgh 2007; Karl et al. 2008).

In the Subarctic and Arctic shelf areas, however, shallow water depths and seasonal sea ice cover complicate the picture. High concentrations of methane have been reported from the entire water column up to the surface (Damm et al. 2008; Shakhova et al. 2010; Mau et al. 2013). In addition, during periods of near 100% sea ice concentrations, the gas exchange from the water column to the atmosphere is restricted (Loose et al. 2011). Under these conditions, maximal dissolved methane concentrations of 5000 nmol L<sup>-1</sup>, or an oversaturation of 160,000% with regard to atmospheric equilibrium, have been reported from the Siberian Shelf (Shakhova et al. 2010).

\*Correspondence: [cuhlig@uri.edu](mailto:cuhlig@uri.edu)

Additional Supporting Information may be found in the online version of this article.

**Data availability statement:** Data were deposited in PANGAEA under doi.pangaea.de/10.1594/PANGAEA.874893. R code for data processing and the sensitivity study is available on GitHub (<https://github.com/cuhlig/ISMOFI/>).

This is an open access article under the terms of the Creative Commons Attribution License, which permits use, distribution and reproduction in any medium, provided the original work is properly cited.

Besides others factors like oxygen and trace metal availability (Sansone et al. 2001; Semrau et al. 2010; Crespo-Medina et al. 2014), the dissolved methane concentration is an important control on the community of methane oxidizing bacteria and thus methane oxidation rates (Kessler et al. 2011; Mau et al. 2013; Crespo-Medina et al. 2014). Methane hotspots, promoted by limited gas exchange under sea ice, might thus be candidate regions for accumulation of methane oxidizers and high methane oxidation rates. Studies on methane oxidation rates in this difficult accessible environment are missing up to date (James et al. 2016).

Methane oxidation rates ( $r_{ox}$ ), expressed as amount of methane oxidized per unit time, have been determined by different indirect and direct methods in aquatic systems. The mass balance of methane has been used to determine oxidation rates from water collected in estuaries, glacier runoff, and lakes (Abril et al. 2007; Dieser et al. 2014; Ricão Canelhas et al. 2016). In these ex situ incubations, CH<sub>4</sub> concentrations were either naturally high or spiked to  $\mu$ molar levels. Scranton and Brewer (1978) correlated methane concentrations with water mass age to determine long term oxidation rates in the deep ocean.

In the last decade, radioisotope tracers—<sup>14</sup>C and/or <sup>3</sup>H labeled methane—have been established as sensitive method to measure oxidation rates in the oceanic water column, where methane concentrations are often low (Valentine et al. 2001; Mau et al. 2012, 2013; Pack et al. 2015). The addition of the radioisotope spike varies between studies ranging from sub-picomolar (Pack et al. 2015) to high nanomolar concentrations (Valentine et al. 2001; Mau et al. 2012, 2013; Pack et al. 2015; reviewed by Bussmann et al. 2015). While the low concentration additions do not disturb the methane concentrations compared to in situ conditions, the higher ones lead to increases of up to 200 times. Despite the apparent advantages, the use of radioisotopes can be complicated due to regulations regarding the transport, handling and need of special laboratory facilities (Bussmann et al. 2015); particularly in remote field sites and across borders.

Stable carbon isotope techniques make use of isotopic fractionation during metabolic processes. Metabolic processes preferably use the lighter carbon isotope over the heavier isotope, leading to fractionation of the residual pool toward heavier isotope ratios (Whiticar 1999). During aerobic methane oxidation methane serves as substrate, being used as an energy and carbon source by the methanotrophs. Microbial oxidation of methane results in both a decrease in the methane concentration and an enrichment of the residual methane with <sup>13</sup>C-CH<sub>4</sub> as well as a depletion of the <sup>13</sup>C in the CO<sub>2</sub> pool. Stable carbon isotope ratios are usually determined with gas chromatography combustion isotope ratio mass spectrometry. These systems have the advantage of having a high precision, but their utility is restricted by their large size, sensitivity to the environmental conditions (e.g., temperature and humidity), and their high cost.

Stable isotope ratios of natural (not incubated) samples have been used to infer the production and oxidation history of the residual methane pool (Whiticar 1999; Sansone et al. 2001; Grant and Whiticar 2002; Damm et al. 2008), or to calculate oxidation rates directly (Bastviken et al. 2002; Leonte et al. 2017). Two recently published studies make use of stable isotopes to measure methane oxidation rates in ex situ incubations of natural seawater (Chan et al. 2016; Leonte et al. 2017). Leonte et al. (2017) use glass bottles with volumes of 160 mL and a pure <sup>13</sup>CH<sub>4</sub> spike at a final concentration of 12  $\mu$ mol L<sup>-1</sup>. Oxidation rates are calculated from changes in the stable carbon isotope ratio of the dissolved inorganic carbon pool. Chan et al. (2016) report the use of large volume (15 L) custom made film bags in a closed system with a Picarro G2201-*i* cavity ring-down spectrometer as mesocosm experiments. A pure <sup>13</sup>CH<sub>4</sub> spike at a final concentration of 300–500  $\mu$ mol L<sup>-1</sup> was added to follow methane conversion processes by changes in the methane concentration and isotope ratios.

Our study reports the use of methane, with a defined stable carbon isotope ratio, as spike in incubation experiments, to measure microbial methane oxidation between nanomolar and low micromolar concentrations. A Picarro G2201-*i* cavity ring-down spectrometer in combination with a Small Sample Isotope Module 2 (SSIM) was used to determine methane concentrations and isotope ratios. The cavity ring-down spectrometer is a benchtop instrument that can easily be transported to and operated in locations like ships and laboratories at field sites. Stable isotope infrared spectroscopy to detect methane oxidation in foil incubators (ISMOFI) circumvents the use of explosive gases (e.g. hydrogen) and toxic chemicals, to facilitate the use in remote locations. Incubations were performed in 1 L multi-layer foil gas sampling bags which allow for several subsequent samplings from the same replicate, due to the large headspace volume and compressibility of the bag.

The aim of this study is to (1) evaluate the use of gas tight foil bags as sample containers for time series studies with the headspace method, (2) introduce the Picarro G2201-*i* benchtop cavity ring-down spectrometer for the determination of methane concentrations and isotope ratios in discrete seawater over a wide range of concentrations, and (3) determine methane oxidation rates from isotope ratios and compare those to oxidation rates determined from mass balance.

## Materials and procedures

### Use of multi-layer foil gas sampling bags

Multi-layer foil gas sampling bags equipped with a polypropylene combo valve and septum (capacity 1000 mL, # 22950, Restek, Bellfonte, Pennsylvania, U.S.A.) were used as sample vessels. Our experiments were performed with approximately 0.8 L seawater and a headspace of 0.1 L permitting for multiple sample extractions from the same sample container in a time series. Besides the large sample

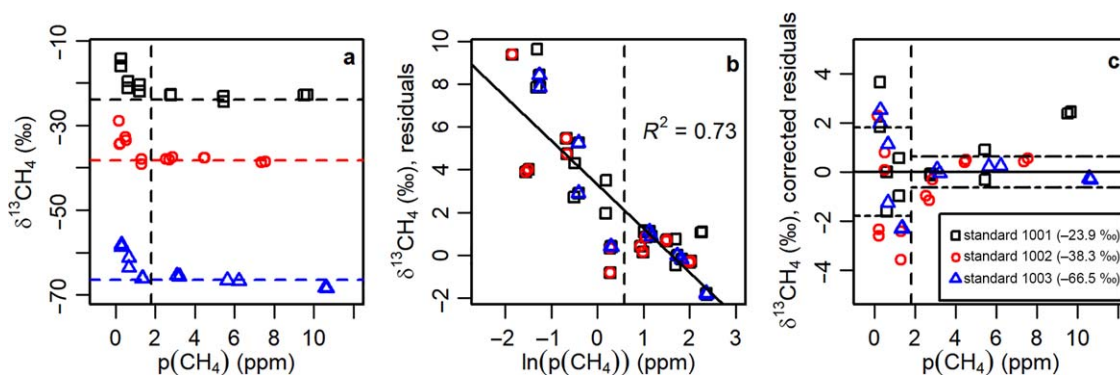


**Fig. 1.** G2201-*i* behavior for isotope ratios ( $\delta^{13}\text{CH}_4$ ) at partial pressures ( $p(\text{CH}_4)$ ) below 12 ppm. **(a)**  $\delta^{13}\text{CH}_4$  vs.  $p(\text{CH}_4)$ . Horizontal dashed lines indicate nominal  $\delta^{13}\text{CH}_4$  of the respective standard. **(b)**  $\delta^{13}\text{CH}_4$  residuals (difference between nominal  $\delta^{13}\text{CH}_4$  and measurement) vs.  $\ln(p(\text{CH}_4))$ . The solid black line shows the logarithmic fit  $\Delta\delta^{13}\text{CH}_4 = -2.05 \times \ln(p(\text{CH}_4)_{\text{injected}}) + 3.31$  ( $R^2 = 0.73$ ,  $n = 38$ ). **(c)** Scatter of the corrected residuals around the fit shown in **(b)**. The horizontal dotted lines show the precision calculated as the mean absolute corrected residuals below and above 1.8 ppm. Precision is 1.8‰ below 1.8 ppm and 0.62‰ above 1.8 ppm. **(a, b, c)** Vertical dashed line is drawn at 1.8 ppm  $\text{CH}_4$ . Black squares, standard 1001  $-23.9 \pm 0.2$ ‰; Red circles, standard 1002  $-38.3 \pm 0.2$ ‰; Blue triangles, standard 1003  $-66.5 \pm 0.2$ ‰.

volume a further advantage is the compressibility of the bag; as long as the bag is not initially overfilled, the internal headspace pressure equals atmospheric pressure at any time, thus not altering the solubility equilibrium.

A potential tradeoff in using these bags is the permeability of the multi-layer foil for low molecular weight gases. Storage experiments were performed with the same type of bag with 3 L volume, to determine the loss of  $\text{CH}_4$  and possible isotopic fractionation. The bags were filled with a gas mixture of  $\text{N}_2$  (ultra high purity (UHP) grade, Airgas, Warwick, Rhode Island) and gas standards of known isotopic composition ( $\delta^{13}\text{CH}_4$   $-23.9 \pm 0.2$ ‰,  $-38.3 \pm 0.2$ ‰, and  $-66.5 \pm 0.2$ ‰, Isometrics, Victoria, British Columbia, Canada) at mixing ratios [ $p(\text{CH}_4)$ ] of approximately 15–35 ppm  $\text{CH}_4$ . Bags were analyzed for  $p(\text{CH}_4)$  and isotopic signature ( $\delta^{13}\text{CH}_4$ ) directly after preparation. Analysis of the same bags was repeated after storage for 48 d and 280 d at room temperature in the dark.

### Measurement of $p(\text{CH}_4)$ and $\delta^{13}\text{CH}_4$

Analysis for  $p(\text{CH}_4)$  and  $\delta^{13}\text{CH}_4$  were performed with a Picarro G2201-*i* cavity ring-down spectrometer (Picarro, Santa Clara, California, U.S.A.) coupled to a SSIM (Picarro, Santa Clara, California, U.S.A.) (Supporting Information Fig. 1). The SSIM is a sample inlet system recommended for determination of isotope ratios from discrete samples as opposed to the continuous measurement of the analyzer itself with a flow rate of approximately  $25 \text{ mL min}^{-1}$ . The SSIM further offers the possibility to dilute highly concentrated samples with hydrocarbon free zero air to reach the specification range of the analyzer of 1.8–500 ppm  $\text{CH}_4$ .

The dilution factor can be calculated from the volume of sample ( $V_{\text{sample}}$ ), volume of the dilution chamber ( $V_{\text{SSIM}} = 20 \text{ mL}$ ), the pressure of the dilution gas ( $P_{\text{SSIM}}$ ), and the atmospheric pressure ( $P_{\text{atm}}$ ):

$$\text{dil}_{\text{SSIM}} = \frac{P_{\text{SSIM}}}{\frac{V_{\text{sample}}}{V_{\text{SSIM}}} \times P_{\text{atm}}} \quad (1)$$

The atmospheric pressure was recorded from a Paroscientific Digiquartz Barometer from 16 April onward (see section “Study Site”). Before this date surface air pressure data from the NOAA Utqiagvik Observatory (<http://www.esrl.noaa.gov/gmd/obop/brw/> 71.323°N, 156.6114°W) was used. Corrections were made with air pressure records from the morning.

To absorb water droplets during injection, the inlet of the SSIM was equipped with a 5 cm long transparent glass tube containing dry tissue (Kimwipe<sup>®</sup>, Kimberly Clark Professional, Georgia, U.S.A.) as absorbent material for experiments performed in Utqiagvik. Afterward, samples were introduced into the SSIM through a Nafion<sup>®</sup> tube in a Permapure Gas Dryer cartridge filled with desiccant (#DM-060-24-COMP2, Permapure LLC, New Jersey, U.S.A.) to absorb water vapor. Sample and standard volumes between 0.02 mL and 10 mL were injected into the SSIM using SGE gastight syringes equipped with shutoff valves (100  $\mu\text{L}$ , 1 mL, 5 mL, 20 mL total volume; SGE, Victoria, Australia). The SSIM coordinator software was run on fast measurement mode, syringe injection setting, and dilution with hydrocarbon free air.

### Corrections and calibrations

The manufacturer recommends the use of the G2201-*i* for methane mixing ratios  $\geq 1.8$  ppm. For mixing ratios below 1.8 ppm, we observed an “amount effect”, leading to the overestimation of the isotope ratio (Fig. 1a). To characterize this effect, standard gases of isotope ratios of  $-23.9$ ‰,  $-38.3$ ‰, and  $-66.5$ ‰ (Isometrics, Victoria, British Columbia, Canada) were introduced into the SSIM with variable syringe volumes to produce mixing ratios between 0.05 ppm and 11 ppm  $\text{CH}_4$ . We observed a regular and highly reproducible behavior in the deviation of the measured from the

**Table 1.** Approximate concentrations of CH<sub>4</sub> in the water ( $c(\text{CH}_4)_{\text{water}}$ ), partial pressures in the headspace of the bag/bottle ( $p(\text{CH}_4)_{\text{hs}}$ ), and inside the analyzer ( $p(\text{CH}_4)_{\text{Pic}}$ ) for Utqiagvik treatments and isotope ratios ( $\delta^{13}\text{CH}_4$ ) in the respective treatment.

Treatment	$c(\text{CH}_4)_{\text{water}}$ (nmol L <sup>-1</sup> )	$p(\text{CH}_4)_{\text{hs}}$ (ppm)	$p(\text{CH}_4)_{\text{Pic}}$ (ppm)	$\delta^{13}\text{CH}_4$ (‰)
0.2×	3	2.5	1.2	-40
0.2× EL	12	6	2.5	-70
2×	35	19	4	-36
10×	100	50	7	-35
200×	4000	1500	65	-23
3× crimp	50	40	1	-38
20× crimp	400	350	1.5	-20

expected isotope ratio ( $\Delta\delta^{13}\text{CH}_4$ ) as a function of the methane mixing ratio. A linear regression of the  $\Delta\delta^{13}\text{CH}_4$  to the logarithm of methane mixing ratio  $\ln(p(\text{CH}_4))$  produced the best fit and was used as empirical correction for standard and sample measurements (Fig. 1b). Measurements resulting in a partial pressure  $p(^{12+13}\text{CH}_4)$  (sum of <sup>13</sup>C and <sup>12</sup>C isotopologues) below 1.8 ppm were corrected as follows:

$$\delta^{13}\text{CH}_4, \text{corrected} = \delta^{13}\text{CH}_4, \text{measured} - \Delta\delta^{13}\text{CH}_4 \quad (2)$$

and

$$\Delta\delta^{13}\text{CH}_4 = m_{\text{fit}} \times \ln(p(^{12+13}\text{CH}_4)) + a_{\text{fit}} \quad (3)$$

with  $\Delta\delta^{13}\text{CH}_4$  being the isotope ratio residuals,  $m_{\text{fit}}$  the slope of logarithmic empirical fit,  $a_{\text{fit}}$  the  $y$ -intercept of logarithmic empirical fit.

Further, standard gases were used to generate linear calibrations for mixing ratios and isotope ratios in order to correct for any transient deviations in the G2201-*i* analyzer. Typically, a calibration was generated every 24 h. The largest batch of measurements between calibrations spanned a time of 31 h. For preparation of the standard curve, gases of known mixing ratio (240–2698 ppm, standard error 2%) and isotope ratio ( $\delta^{13}\text{CH}_4$  -23.9‰ to -66.5‰) were used in at least two different mixing and isotope ratios to bracket the sample data. We calculated separate standard curves for the high precision (HP) and high dynamic range (HR) mode of the analyzer. Some calibration curves had to be rejected due to problems during data acquisition (e.g., carry over, memory effects of preceding samples). In these cases, the closest neighboring calibration was used.

### Study site

Arctic seawater was collected at two sites close to Utqiagvik, North Slope, Alaska on 07 April 2016, 09 April 2016, and 15 April 2016 in the Beaufort Sea. Site “Elson Lagoon” (EL) was located North of Utqiagvik (07.04.2016, 71.334° N, -156.363° W), covered with 1.5 m thick sea ice and shallow with approximately 1.5 m depth. Water was collected from a depth of 1.5 m in a narrow layer of water between the sea ice and the sediment. Site “Ice Mass Balance Buoy” (IMB) was located

1 km offshore of Utqiagvik, close to the IMB of the sea ice physics group of University of Alaska, Fairbanks (07.04.2016, 71.373° N, -156.548° W, and 09.04.2016, 71.372° N, -156.540° W). This site was characterized by 1 m thick fast ice cover and a water depth of approximately 7 m. Water was collected at five depth from 1 m to 6.5 m. Similar to other shallow shelf areas, at our study site, CH<sub>4</sub> is possibly released to the water column from the anoxic sediments and geological storages (Kvenvolden et al. 1993; Shakhova et al. 2010). At both sampling sites, CH<sub>4</sub> introduction by submarine groundwater discharge was reported to add to the other CH<sub>4</sub> sources (Lecher et al. 2016). Under ice cover, water CH<sub>4</sub> concentrations in Utqiagvik were reported to reach maximum concentrations of 116.4 nmol L<sup>-1</sup>, a supersaturation of 3100% with regard to atmospheric equilibrium (Zhou et al. 2014).

Additionally, seawater was sampled in Narragansett Bay (Nbay), Rhode Island (41.492° N, -71.419° W) on 15 July 2016 to test our method for applicability under different environmental conditions. Sampling depth was 2–3 m at a water depth of approximately 6 m with water temperature of 20.5°C and salinity of 33.1.

### Incubation experiments

Microbial oxidation of methane was investigated with incubations of seawater in gas tight foil bags. Using a peristaltic pump (Masterflex Environmental Sampler, Cole Parmer, Illinois, U.S.A.) or submersible pump (Cyclone, Proactive Environmental Products, Florida, U.S.A.), 0.7–0.9 L seawater was transferred bubble free into 1 L sampling bags in the field. Upon return to the laboratory a 0.1 L headspace of hydrocarbon free air (zero air, Air Liquide, Anchorage, Alaska) was introduced into the bags through the septum using a 100 mL glass syringe (Fortuna® All Glass Syringes, Air-Tite Products, Virginia). The bags were additionally spiked with a stable isotope methane tracer (Isometrics, Victoria, British Columbia, Canada) to result in different concentrations and isotopic signatures (Table 1). One replicate of the Utqiagvik incubations was treated with 10 mL 10 M sodium hydroxide (NaOH) and served as killed control. The bags were incubated for 6–45 d and the headspace repeatedly sampled to follow methane concentrations and isotope

ratios. Incubation experiments in Utqiagvik were incubated in an ice bath made from a freshwater and snow mixture at 0°C in the dark for the first 12 d. Care was taken to submerge the valves in the water, thus creating a hydraulic diffusive barrier in the stem of the valve to guard against any possible leaks in the septum. For transport from Utqiagvik back to our laboratory at the University of Rhode Island, Graduate School of Oceanography (URI/GSO), the valve stems were filled with water and sealed with tape to create the same effect. They were transported via airplane in a Styrofoam cooler as luggage and arrived at their destination with a temperature of 0°C. Afterward, samples were stored at 1°C in the dark, but were not submerged into a water bath.

Prior to each measurement, the headspace and water were allowed to equilibrate for at least 12 h. Additionally, the bags were shaken by hand for approximately 2 min before retrieving a sample from the headspace. The bags were kept on ice during handling to avoid an increase in water temperature.

A second set of incubation experiments was prepared as described above from water sampled in Utqiagvik into 4 L foldable low density polyethylene (LDPE) canisters (Hedwin, Delaware, U.S.A.) and transported to the laboratory at URI/GSO. The water was stored at 1°C for 12 weeks in the dark before setting up the experiments.

Last, a third batch was set up from water sampled in Naragansett Bay in July 2016. These experiments were prepared similar to the Arctic water incubations, but were kept at a temperature of 18°C. Both of the experimental sets prepared at URI/GSO were incubated in a water bath with valves submerged over the entire duration of the experiment. A total of five NaOH killed controls were set up for the experiments performed at URI/GSO.

Dissolved oxygen was determined with an YSI Professional Plus probe (YSI, Ohio, U.S.A.) or SBE 37-SMP-ODO MicroCAT C-T-ODO (P) Recorder (Sea-Bird Electronics, Washington, U.S.A.) during fieldwork and at the end of the incubation experiments.

#### Oxidation rates from mass balance

Microbial oxidation of methane in a closed reservoir will result in a decrease of bulk methane and thus methane concentration within the reservoir. In our experimental setup, the reservoir of methane ( $n(\text{CH}_4)_{\text{total}}$ ) is the sum of the mass of methane dissolved in the water ( $n(\text{CH}_4)_{\text{w}}$ ) and the mass of methane in the headspace ( $n(\text{CH}_4)_{\text{hs}}$ ) in moles.

$$n(\text{CH}_4)_{\text{total}} = n(\text{CH}_4)_{\text{w}} + n(\text{CH}_4)_{\text{hs}} \quad (4)$$

Oxidation by bacteria will consume  $\text{CH}_4$  dissolved in the water. In addition, the removal of a sample will reduce the  $\text{CH}_4$  reservoir in the headspace at a given time ( $t = i - 1$ ). The decrease in the headspace volume effectively decreases the moles of methane that can transfer to the water for oxidation. Before calculating the oxidation rate, the total mass of

$\text{CH}_4$  was corrected for the mass removed during sampling to obtain  $n(\text{CH}_4)_{\text{total, corrected}}$  (details in Appendix A).

It is customary to assume that microbial methane oxidation can be modeled as a first order kinetic process during the exponential oxidation phase (Reeburgh et al. 1991; Valentine et al. 2001).

$$\ln \left( \frac{n(\text{CH}_4)_{\text{total, corrected}, t_i}}{n(\text{CH}_4)_{\text{total, corrected}, t_{i-1}}} \right) = -k_{\text{ox, ppm}} \times t_{i-(i-1)} \quad (5)$$

where  $n(\text{CH}_4)_{\text{total, corrected}, t_i}$  was calculated as

$$n(\text{CH}_4)_{\text{total, corrected}, t_i} = n(\text{CH}_4)_{\text{total}, t_i} + \sum_{j=0}^{j=t_i-1} n(\text{CH}_4)_{\text{sampled}} \quad (6)$$

Therefore, the oxidation rate constant  $k_{\text{ox}}$  (with units of  $\text{time}^{-1}$ ) can be determined as the negative slope of the linear regression of  $\ln \left( n(\text{CH}_4)_{\text{total, corrected}} \right)$  and the incubation time ( $t_i$ ). Conventionally, a positive  $k_{\text{ox}}$  indicates a decrease in methane concentration, while a negative  $k_{\text{ox}}$  indicates an increase.

Molar quantities of methane in the headspace ( $n(\text{CH}_4)_{\text{hs}}$ ) and water ( $n(\text{CH}_4)_{\text{w}}$ ) were calculated as equilibrium concentrations according to Magen et al. (2014) with the equilibrium constant according to Yamamoto et al. (1976). Finally, the rate of bacterial methane oxidation  $r_{\text{ox}}$  was determined as the product of the oxidation rate constant and the in situ concentration of  $\text{CH}_4$  dissolved in the water ( $c(\text{CH}_4)_{\text{w, in situ}}$ ).

$$r_{\text{ox}} = k_{\text{ox}} \times c(\text{CH}_4)_{\text{w, in situ}} \quad (7)$$

#### Oxidation rates from isotopic fractionation

In addition to the decrease in the total mass of  $\text{CH}_4$  caused by microbial oxidation of  $\text{CH}_4$ , the carbon isotope ratio of the remaining methane pool changes due to isotopic fractionation (Whiticar 1999). Mahieu et al. (2006) develop the simplified Rayleigh model

$$\ln(f) \left( \frac{1}{\alpha_{\text{ox}}} - 1 \right) = \ln \left( \frac{1000 + \delta^{13}\text{CH}_4 t_i}{1000 + \delta^{13}\text{CH}_4 t_0} \right) \quad (8)$$

where  $f = n(\text{CH}_4 t_i) / n(\text{CH}_4 t_0)$  and isotope ratios are described in  $\delta$ -notation

$$\delta^{13}\text{C} = \frac{R_{\text{sample}}}{R_{\text{standard}}} - 1 \quad (9)$$

and  $R$  describes the isotope ratio of  $^{13}\text{CH}_4 / ^{12}\text{CH}_4$  in the sample and standard (Vienna Peedee Belemnite, McKinney et al. 1950), respectively.

The fractionation factor  $\alpha_{\text{ox}} = k_{12} / k_{13}$  (Mahieu et al. 2006) is the ratio of the kinetic constants for reactions of the heavier ( $k_{13}$ ) and lighter ( $k_{12}$ ) isotope  $\text{CH}_4$  (Appendix B).

Combining Eq. 8 with the first order kinetics (Eq. 5), we get

**Table 2.** Diffusive loss rates of O<sub>2</sub>, CO<sub>2</sub>, and CH<sub>4</sub> from multi-layer foil gas sampling bags.

	Diffusive loss rate	Source
O <sub>2</sub>	$0.6 \times 10^{-3} \text{ mL m}^{-2} \text{ d}^{-1}$	Manufacturer
CO <sub>2</sub>	$7.7 \times 10^{-3} \text{ mL m}^{-2} \text{ d}^{-1}$	Manufacturer
CH <sub>4</sub>	$7.8 \times 10^{-5} \text{ to } 8.3 \times 10^{-3} \text{ mL m}^{-2} \text{ d}^{-1}$	This study
$\delta^{13}\text{CH}_4$	No significant change	—

$$-k_{\text{ox,delta}} \times t = \frac{\ln\left(\frac{1000 + \delta^{13}\text{CH}_{4\text{ti}}}{1000 + \delta^{13}\text{CH}_{4\text{t0}}}\right)}{\left(\frac{1}{\alpha_{\text{ox}}} - 1\right)} \quad (10)$$

where  $\delta^{13}\text{CH}_{4\text{ti}}$  is the isotope ratio corrected for the empirical correction if  $p(\text{CH}_4) < 1.8 \text{ ppm}$  as well as the respective calibration.

By plotting  $\ln\left(\frac{1000 + \delta^{13}\text{CH}_{4\text{ti}}}{1000 + \delta^{13}\text{CH}_{4\text{t0}}}\right) / \left(\frac{1}{\alpha_{\text{ox}}} - 1\right)$  vs.  $t$ , the first order oxidation rate constant derived from  $\delta^{13}\text{CH}_4$  ( $k_{\text{ox,delta}}$ ) can be determined as the negative slope of the linear regression. Where a positive  $k_{\text{ox,delta}}$  indicates an increase in  $\delta^{13}\text{CH}_4$ , and a negative  $k_{\text{ox,delta}}$  a decrease. Fractionation factors reported from cold marine environments with temperatures below 2°C (e.g., cold and hydrothermal plumes, Arctic seawater) lie in the range of 1.002–1.017 (Cowen et al. 2002; Grant and Whiticar 2002; Damm et al. 2007; Fenwick et al. 2017). Since these values were calculated from in situ data, they might be underestimated due to mixing effects in the water column (Grant and Whiticar 2002). In this study, we use  $\alpha_{\text{ox}}$  of 1.007 and 1.025 as lower and upper bounds. Oxidation rates were determined according to Eq. 7 using  $k_{\text{ox,delta}}$  with  $\alpha_{\text{ox}} = 1.025$ .

Isotopic fractionation occurring during dissolution of methane from the headspace into the water is a factor of 10 lower (Fuex 1980). It acts opposite to the fractionation during methane oxidation and might lead to a slight underestimation of  $k_{\text{ox,delta}}$  (Supporting Information Material).

### Statistics

Calibration, post-processing, and analyses were performed with the software package R version 3.2.3 in RStudio Version 0.99.903. Plots were prepared with base and ggplot2 packages. Each linear regressions for determination of  $k_{\text{ox,ppm}}$  and  $k_{\text{ox,delta}}$  was tested for its difference from zero at 95% confidence level (build in  $t$ -test, R base). In addition, both oxidation rate constants ( $k_{\text{ox,ppm}}$  vs.  $k_{\text{ox,delta}}$ ) were compared to each other applying Welch's  $t$ -test (Welch 1938; Andrade and Estévez-Pérez 2014, Eqs. 5, 5c).

### Assessment

#### Use of multi-layer foil bags

Diffusive loss of CH<sub>4</sub> through the gas sampling bags stored in air was determined by repeated measurement of three gas mixtures after storage for 1 d, 48 d, and 280 d. We observed a diffusive loss rate constant  $k_{\text{diff}}$  of  $3.6 \times 10^{-4} \text{ d}^{-1}$

( $\pm 6.2 \times 10^{-4}$ ,  $n = 3$ ) at 14–34 ppm resulting in a loss of  $7.8 \times 10^{-5}$  to  $8.3 \times 10^{-3} \text{ mL CH}_4 \text{ m}^{-2} \text{ d}^{-1}$  for CH<sub>4</sub> mixing ratios of 14 ppm and 1500 ppm, respectively (Table 2). Changes in isotope ratios were within measurement uncertainties.

In addition, the first order rate constants ( $k_{\text{ox}}$ ) of our NaOH treated killed controls during the incubation experiments provide an estimate of diffusive or other nonbiological methane loss under experimental conditions. In the killed controls,  $k_{\text{ox,ppm}}$  was  $-1.8 \times 10^{-3} \pm 6.0 \times 10^{-3}$  ( $n = 6$ ,  $2.8 \times 10^{-3} \text{ d}^{-1}$  to  $-1.4 \times 10^{-2} \text{ d}^{-1}$ ) at mixing ratios of 19–15,000 ppm in the headspace. For only two out of the six replicates, the slopes of the regressions were significantly different from 0 at a 95% confidence level. Changes in  $\delta^{13}\text{CH}_4$  were one order of magnitude lower with  $k_{\text{ox,delta}}$  of  $-3.7 \times 10^{-4}$  ( $n = 6$ , with one out of six significantly different from 0).

The bags were reused for a maximum of two times after inspection for damage, cleaning with ethanol and replacing the septum (full procedure in Supporting Information Materials and Methods). Our 50 incubations did not show evidence for major inconsistent leaks, except for the entire and obvious loss of two bags during transport.

### Determining experimental uncertainty

To estimate the variability of our measurements, subsequent corrections and calculations each data point was determined in two to seven technical replicates. The mean standard deviation for replicates of the final calibrated sample data is displayed in Table 3. Relative and absolute deviation between replicate samples was lower for replicates the HR mode (12–500 ppm CH<sub>4</sub>) than in the HP range ( $< 12 \text{ ppm CH}_4$ ). The mean relative standard deviation was below or equal to  $2.02\% \pm 3.85\%$  for  $c(\text{CH}_4)_{\text{water}}$  and  $0.73\% \pm 1.51\%$  for  $\delta^{13}\text{CH}_4$  in both measurement ranges.

The variance ( $\sigma_y^2$ ) on calibrated data ( $y$ ) with  $y = mx + b$  was calculated as propagated error of the slope ( $m$ ) and intercept ( $b$ ) of the calibration curve with the measured values ( $y$ ) using Taylor expansion according to the following equation:

$$\sigma_y^2 = \sigma_m^2 x^2 + \sigma_x^2 m^2 + \sigma_b^2 + 2\sigma_{bm} x^2 \quad (11)$$

Further covariance terms equal 0 since the errors on  $x$  and  $m$  as well as  $x$  and  $b$  are unrelated, resulting in  $\sigma_{xm}^2 = 0$  and  $\sigma_{xb}^2 = 0$ . The resulting standard deviation ( $\sqrt{\sigma_y^2}$ ) for the HP mode was  $4.24\% \pm 1.68\%$  for the concentration and  $4.33\% \pm 2.38\%$  for the isotope ratio, while for the HR mode slightly lower errors of respectively  $3.82\% \pm 1.76\%$  and  $3.22\% \pm 2.06\%$  were determined (Supporting Information Table 1).

To assess the performance of the empirical correction of samples with low methane concentration we reevaluated the precision of the isotope ratios measurements after applying the correction. The precision was calculated as the mean absolute deviation of the measured value from the empirical

**Table 3.** Mean of standard deviation (mean SD) on concentrations of CH<sub>4</sub> in the water ( $c(\text{CH}_4)_{\text{water}}$ ) and isotope ratios ( $\delta^{13}\text{CH}_4$ ) of final calibrated data for the two measurement modes of the G2201-*i*. The number of replicate sets is given as  $n$ , while each set had 2–7 data points. Deviations are given as absolute (nmol/L, ‰) and relative (%) values.

Dataset	$n$	$c(\text{CH}_4)_{\text{water}}$		$\delta^{13}\text{C}$ calibrated	
		Mean SD (nmol/L)	Mean SD %	Mean SD (‰)	Mean SD %
<b>HP mode*</b>					
Utqiagvik	81	$0.97 \pm 1.33$	$1.61 \pm 1.96$	$0.33 \pm 0.53$	$0.73 \pm 1.51$
Home lab	110	$1.19 \pm 1.92$	$2.02 \pm 3.85$	$0.45 \pm 1.59$	$0.37 \pm 2.63$
<b>HR mode*</b>					
Utqiagvik	39	$44.53 \pm 90.97$	$1.16 \pm 2.22$	$0.06 \pm 0.07$	$0.27 \pm 0.28$
Home lab	35	$41.48 \pm 51.75$	$1.37 \pm 2.03$	$0.09 \pm 0.27$	$0.38 \pm 1.17$

\*HP mode: 1.8–12 ppm, HR mode: 12–500 ppm.

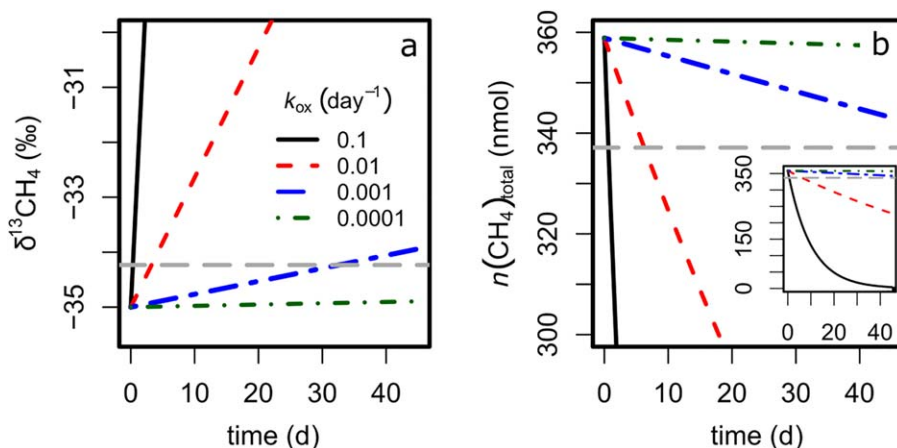


**Fig. 2.** Sensitivity of  $\delta^{13}\text{CH}_4$  (a) and  $n(\text{CH}_4)_{\text{total}}$  (b) for varying first order oxidation constants ( $k_{\text{ox}}$ ),  $c(\text{CH}_4)_{\text{water,initial}} = 120 \text{ nmol L}^{-1}$  and  $\delta^{13}\text{CH}_4, \text{initial} = -35\text{‰}$  in a model calculation. The gray horizontal lines indicate the sensitivity threshold of 2.2% of the initial value for  $\delta^{13}\text{CH}_4$  and 6.1% for  $n(\text{CH}_4)_{\text{total}}$ . The sensitivity threshold was defined as three times the relative mean standard deviation of replicate measurements (Table 3).

model for mixing ratios  $> 1.8$  ppm, and as the mean absolute deviation of the corrected residuals to the empirical model for mixing ratios  $< 1.8$  ppm (Fig. 1c). The precision of isotope ratios was  $0.62 \pm 0.70\text{‰}$  ( $N = 19$ , mean + one standard deviation) for mixing ratios  $> 1.8$  ppm methane, and  $1.8 \pm 1.04\text{‰}$  ( $N = 19$ ) below  $< 1.8$  ppm (Fig. 1c, Supporting Information Table 1).

#### Detection limits and sensitivity on methane oxidation

The oxidation of methane is determined by the oxidation rate kinetics and the concentration of dissolved methane in the water (see Eq. 7). Using the ISMOFI experimental configuration, we have resolved oxidation constants down to  $0.01 \text{ d}^{-1}$  with high statistical support, which is comparable to  $k_{\text{ox}}$  determined with tritium labeled methane (Mau et al. 2013). Most water bodies in contact with the atmosphere will have methane concentrations which are at equilibrium concentration with air or higher. At Arctic temperatures, the ocean should have a minimum concentration of  $3.8 \text{ nmol L}^{-1}$

CH<sub>4</sub>, which implies an oxidation rate of  $0.038 \text{ nmol L}^{-1} \text{ d}^{-1}$ . This lower limit covers about 80% of the range of oxidation rates ( $0.002\text{--}820 \text{ nmol L}^{-1} \text{ d}^{-1}$ ) published for Arctic and Subarctic environments (Mau et al. 2013; Gentz et al. 2014; Damm et al. 2015; Steinle et al. 2015; Mau et al. 2017) or marine sites with extraordinarily high oxidation rates at oil spills or gas flares (Valentine et al. 2010; Steinle et al. 2016). The lower limit on oxidation rates in the ISMOFI experimental configuration is imposed by the diffusive loss of gas from the foil bag incubators of approximately  $3.6 \times 10^{-4} \text{ d}^{-1}$  or by the first order rate constant ( $k_{\text{ox,ppm}}$ ) of our NaOH killed controls during incubation experiments with  $-1.8 \times 10^{-3} \text{ d}^{-1}$ . Changes in isotope ratios in the killed controls were lower than the concentration changes, suggesting that rates determined by stable isotopes could be more promising to resolve slow oxidation rates.

A sensitivity model was used to test the behavior of the presented method for varying oxidation rate constants ( $k_{\text{ox}}$ ), initial CH<sub>4</sub> concentrations ( $c(\text{CH}_4)_{\text{water,initial}}$ ), and isotope

ratios ( $\delta^{13}\text{CH}_4$ ,<sub>initial</sub>). Varying oxidation rate constants  $k_{\text{ox}}$  have the largest effect on the behavior of the model (Fig. 2, Supporting Information Fig. 2). For  $k_{\text{ox}} = 0.01 \text{ d}^{-1}$ , the change in isotope ratio and mass of the residual methane ( $n(\text{CH}_4)_{\text{total}}$ ) passed the sensitivity threshold after 4 d and 7 d, respectively; for  $k_{\text{ox}} = 0.001 \text{ d}^{-1}$ , the time needed to pass the threshold was 33 d and > 35 d (Fig. 2). The initial isotope ratio has a minor effect on the sensitivity (< 1 d), with more positive isotope ratios fractionating slightly faster. The initial dissolved methane concentration does not affect the sensitivity of our method in the model (data not shown). However, it has to be noted that mixing ratios above 1.8 ppm  $\text{CH}_4$  in the analyzer are advantageous due to the low concentration effects on the isotope ratios.

The duration of the incubations is a major determining factor for the detection limit of our method. The sensitivity study shows that with a long incubation time (> 33 d) rates down to the rate of the diffusive loss rate ( $0.001\text{--}0.005 \text{ d}^{-1}$ ) could be resolved (Fig. 2). However, such a long incubation time may not be representative of in situ conditions. The method is thus better suited for oxidation rate constants  $k_{\text{ox}} \geq 0.01 \text{ d}^{-1}$ .

## Results

### In situ conditions

Water samples from Utqiagvik were taken from beneath a closed fast ice cover.

The concentration at site EL was  $53.20 \text{ nmol L}^{-1}$  ( $n = 1$ ). This is higher than previously reported for ice free conditions (Lecher et al. 2016, mean:  $26 \text{ nmol L}^{-1}$ , range:  $3.3\text{--}124.0 \text{ nmol L}^{-1}$ ,  $n = 23$ ) in EL. The water sampled at five different depths from 1 m to 6.5 m at site IMB was treated as replicates for this study, with  $\text{CH}_4$  concentrations of  $16.35 \pm 7.18 \text{ nmol L}^{-1}$  ( $n = 5$ ). These concentrations are somewhat lower than previously reported for ice free (Lecher et al. 2016, mean:  $40.6 \text{ nmol L}^{-1}$ , range:  $0.0\text{--}251.0 \text{ nmol L}^{-1}$ ,  $n = 69$ ) and ice covered conditions (Zhou et al. 2014, March/April:  $37.5 \pm 6 \text{ nmol L}^{-1}$ , June  $77.4 \pm 27.8 \text{ nmol L}^{-1}$ ) in the same area within 10 km from our study site. In Nbay, the concentration of dissolved methane was  $9.30 \pm 1.97 \text{ nmol L}^{-1}$  ( $n = 2$ ) at the sampling depth of 2–3 m.

These concentration values might slightly underestimate true in situ concentrations. Since samples were equilibrated overnight at  $0^\circ\text{C}$  before measurement and were not fixed, methane oxidation might have taken place during those  $\sim 12 \text{ h}$ .

Oxygen saturations calculated according to Garcia and Gordon (1992) was 95% for site EL and ranged from 86% to 96% at site IMB. We did not record in situ data on oxygen saturation for Narragansett Bay.

### Incubation experiments

The rates of methane oxidation were independently determined from the mass balance of total  $\text{CH}_4$  in the

bags, and from the change in isotope ratio of residual  $\text{CH}_4$  (Fig. 3).

All  $200\times$  treatments showed a decrease in  $n(\text{CH}_4)_{\text{total}}$  and increase  $\delta^{13}\text{CH}_4$  after an initial lag phase of approximately 6 d (Fig. 3a–d). The  $10\times$  incubations behaved different depending on the sampling site. The IMB incubations (Fig. 3e–h) decrease in  $n(\text{CH}_4)_{\text{total}}$  and increase  $\delta^{13}\text{CH}_4$ , but at a slower rate than the  $200\times$  incubations, whereas IMB stored and Narragansett Bay did not show any change. Our NaOH treated negative controls did not exhibit significant changes in either concentration or isotope ratio of  $\text{CH}_4$  (Fig. 3a–d). For treatments  $0.1\times$  and  $2\times$ , we did not resolve significant decrease in  $n(\text{CH}_4)_{\text{total}}$  or increase in  $\delta^{13}\text{CH}_4$  during 6 d incubation time (data not shown). One out of three samples of the Narragansett Bay  $2\times$  treatments, however, showed an increase in  $n(\text{CH}_4)_{\text{total}}$  paired with a decrease in  $\delta^{13}\text{CH}_4$ . Low oxygen saturation of 14% at the end of the experiment as well as a hydrogen sulfide smell indicated anaerobic methane production in this single sample.

For all other samples, oxygen saturations were found to be 85–105% ( $\pm 20\%$ ) at the end of the experiments. The increase in saturation compared to in situ concentration can be explained by the addition of zero air during the incubations.

### Oxidation rate kinetics: comparison of $k_{\text{ox,delta}}$ to $k_{\text{ox,ppm}}$

The first order constants for methane oxidation determined from isotope ratios ( $k_{\text{ox,delta}}$ ) were compared to first order constants for methane oxidation determined from the  $\text{CH}_4$  mass balance ( $k_{\text{ox,ppm}}$ ) (Fig. 4; Table 4). The isotopic fractionation factor  $\alpha_{\text{ox}}$  has a major influence on the accuracy of  $k_{\text{ox,delta}}$  (Eq. 10). In our study,  $k_{\text{ox,delta}}$  was close to  $k_{\text{ox,ppm}}$  for  $\alpha_{\text{ox}} = 1.025$ , while for low  $\alpha_{\text{ox}} = 1.007$ ,  $k_{\text{ox,delta}}$  overestimated the oxidation compared to  $k_{\text{ox,ppm}}$  (Fig. 4a). For all samples with high statistical support on  $k_{\text{ox,ppm}}$  and  $k_{\text{ox,delta}(1.025)}$ , (i.e.,  $k_{\text{ox}} \neq 0$ , Table 4), both oxidation rate constants were statistically different from each other (Welch's *t*-test, 95% confidence level). However, the ratio  $k_{\text{ox,ppm}}/k_{\text{ox,delta}}$  was within a range of 0.6–3.7 for 12 out of 14 samples (Table 4).

Agreement between both methods was further dependent on the concentration of spiked methane and sampling site. The correlation was good for the  $10\times$  treatment ( $k_{\text{ox,ppm}}/k_{\text{ox,delta}} = 0.8$ ), with medium methane concentrations ( $100 \text{ nmol L}^{-1}$ ) and isotope ratios of  $-35\text{‰}$  (Table 1). Standard deviation on  $k_{\text{ox,ppm}}$  and  $k_{\text{ox,delta}}$  was low at these concentrations and statistical support high (Fig. 4b, Table 4, Supporting Information Fig. 3). For the  $200\times$  treatments ( $4000 \text{ nmol L}^{-1}$ ),  $k_{\text{ox,ppm}}$  was slightly higher than  $k_{\text{ox,delta}}$  for IMB and IMB stored incubations, while for Nbay  $k_{\text{ox,delta}}$  showed higher oxidation rate constants (Fig. 4b; Table 4). The differences in  $k_{\text{ox,delta}}$  might indicate different isotopic fractionation factors  $\alpha_{\text{ox}}$  in both systems, driven by different microbial communities or incubation temperatures (IMB:  $0\text{--}1^\circ\text{C}$ , Nbay:  $18^\circ\text{C}$ ). For low methane spike concentrations,  $k_{\text{ox}}$

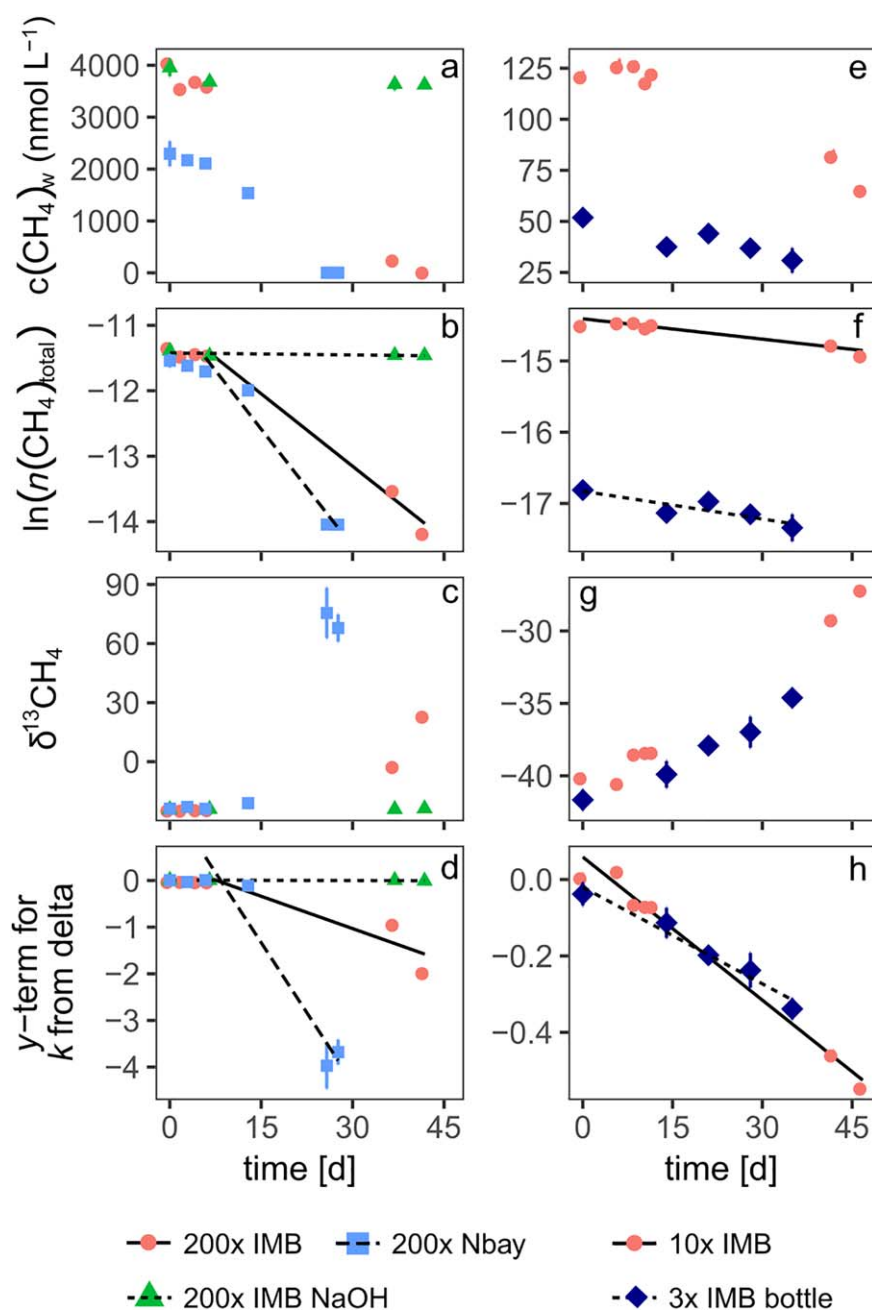


**Fig. 3.** Concentration of  $\text{CH}_4$  in the water ( $c(\text{CH}_4)_{\text{water}}$ ) (**a, e**), natural logarithm of the total molar mass of  $\text{CH}_4$  ( $\ln(n(\text{CH}_4)_t)$ ) (**b, f**), isotope ratio ( $\delta^{13}\text{CH}_4$ ) (**c, g**), and y-axis-term according to Eq. 10 (**d, h**) in selected incubations at  $\text{CH}_4$  spike concentrations of  $200\times$  (**a-d**) and  $10\times/3\times$  (**e-h**). Sampling sites are Utqiagvik, Alaska, close to the IMB and Nbay. The slope of the regression lines in (**b, f**), and (**g, h**) result in the respective  $k_{\text{ox}}$  as described in the text (Eqs. 5, 10). Error bars are standard deviations of technical replicates from one bag and are, if not present, covered by the symbol size.

was either not significant or the rates did not agree between both methods ( $0.2\times$ ,  $2\times$ ; Tables 1, 4). The sensitivity study suggests that the incubation period of 6 d for the  $0.2\times$  and  $2\times$  spike incubations was too short if rate constants were  $<0.01 \text{ d}^{-1}$  (Fig. 2). Negative significant  $k_{\text{ox}}$  was observed with both methods for one out of the three Narragansett Bay  $2\times$  incubations, indicating methane production in this sample (Fig. 4; Table 4).

Logistic constraints lead to a disruption of measurements for the  $10\times$  and  $200\times$  IMB and EL incubations after 6 d. Measurements were resumed on day 38 of the incubations. This makes it difficult to determine if the detection limit from the sensitivity study is met by the incubation experiments. Measurements performed in Rhode Island and on the crimp bottles, however, show that significant changes could be observed within 10 d (Fig. 3).

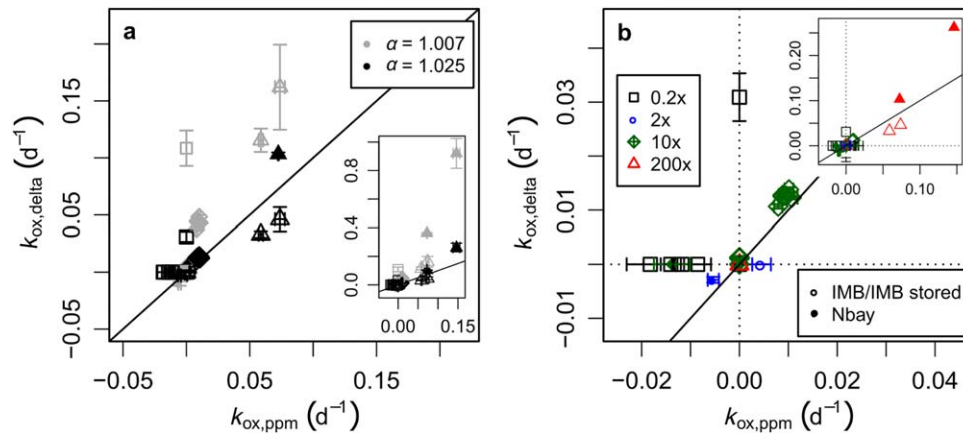


**Fig. 4.** Comparison between first order oxidation constants ( $k_{ox}$ ) determined from  $\text{CH}_4$  concentration (ppm) and isotope ratios (delta). **(a)**  $k_{ox,delta}$  was determined with two different fractionation factors  $\alpha_{ox} = 1.007$  in gray and  $\alpha_{ox} = 1.025$  in black. Black solid line is  $y = x$ . **(b)** Enlarged for  $k_{ox,delta}$  with  $\alpha_{ox} = 1.025$ . Data are subset according to the sampling site; open symbols: Barrow (IMB), filled symbols: Nbay; and methane spike concentrations; black squares: 0.2 $\times$ , blue circles: 2 $\times$ , green diamond: 10 $\times$ , red triangles: 200 $\times$ . Note the different scales on the axes between **(a)** and **(b)**. Error bars indicate the standard error of the slope of the linear models determined according to Eqs. 5, 10.

**Table 4.** Comparison of first order rate constants determined from concentration ( $k_{ox,ppm}$ ) and isotope ratio ( $k_{ox,delta}$ ). Mean of  $k_{ox}$  rates of  $n$  replicates and number ( $N$ ) of test results with  $k_{ox,ppm} = 0$ ,  $k_{ox,delta} = 0$  at 95% confidence level. Mean and standard deviation of the ratio  $k_{ox,ppm}/k_{ox,delta}$ . Positive  $k_{ox}$  indicate a decrease in  $c(\text{CH}_4)_{\text{water}}$  (increase in  $\delta^{13}\text{C}$ ), while a negative  $k_{ox}$  indicate an increase in  $c(\text{CH}_4)_{\text{water}}$  (decrease in  $\delta^{13}\text{C}$ ).

Treatment	$n$	Time (d)	$k_{ox,ppm}$ Mean*	$k_{ox,ppm} = 0$ N*	$k_{ox,delta}$ Mean*	$k_{ox,delta} = 0$ N*	$k_{ox,ppm}/k_{ox,delta}$ Mean $\pm$ SD <sup>†</sup>
<b>Utqiagvik IMB</b>							
0.2 $\times$	5	10	$-1.05 \times 10^{-2}$	1	0	5	n. d.
2 $\times$	4	5	0	4	0	4	n. d.
10 $\times$	5	46	$9.18 \times 10^{-3}$	0	$1.22 \times 10^{-2}$	0	$0.8 \pm 0.07$
200 $\times$ lag	7	6	$1.13 \times 10^{-2}$	3	$1.41 \times 10^{-3}$	2	n. d.
200 $\times$ long	2	41	$6.62 \times 10^{-2}$	0	$3.95 \times 10^{-2}$	0	$1.7 \pm 0.1$
200 $\times$ NaOH	1	41	0	1	0	1	n. d.
3 $\times$ crimp	1	35	$1.37 \times 10^{-2}$	1	$8.33 \times 10^{-3}$	0	1.6
20 $\times$ crimp	1	42	$7.62 \times 10^{-2}$	0	$5.68 \times 10^{-2}$	0	1.3
<b>Utqiagvik EL</b>							
0.2 $\times$	1	10	0	1	$3.09 \times 10^{-2}$	0	n. d.
10 $\times$	1	46	$1.01 \times 10^{-2}$	0	$1.38 \times 10^{-2}$	0	0.7
<b>Utqiagvik IMB stored</b>							
2 $\times$	3	45	$1.51 \times 10^{-3}$	2	0	3	n. d.
10 $\times$	3	45	0	2	$1.22 \times 10^{-3}$	0	n. d.
200 $\times$	3	45	$7.14 \times 10^{-3}$	0	$1.25 \times 10^{-3}$	0	$2.7, 4.7, -13.6$ <sup>‡</sup>
2 $\times$ NaOH	1	45	0	1	0	1	n. d.
10 $\times$ NaOH	1	45	0	1	0	1	n. d.
200 $\times$ NaOH	1	45	$2.77 \times 10^{-3}$	0	$-3.73 \times 10^{-4}$	0	-7.4
<b>Narragansett Bay</b>							
2 $\times$	3	45	$-1.77 \times 10^{-3}$	2	$-9.55 \times 10^{-4}$	2	1.9, n. d., n. d. <sup>‡</sup>
10 $\times$	3	45	0	3	0	3	n. d.
200 $\times$	2	27	$1.09 \times 10^{-1}$	0	$1.83 \times 10^{-1}$	0	$0.6 \pm 0.1$
2 $\times$ NaOH	1	45	$-1.38 \times 10^{-2}$	0	0	1	n. d.
10 $\times$ NaOH	1	45	0	1	0	1	n. d.

\*For calculation of the mean,  $k_{ox}$  was set to zero if the slope from the linear model was not significantly different from zero at a 95% confidence level.

<sup>†</sup> $k_{ox,ppm}/k_{ox,delta}$  was calculated only for samples with  $k_{ox} \neq 0$ .

<sup>‡</sup>Separate values given instead of mean  $\pm$  SD, due to high variability.

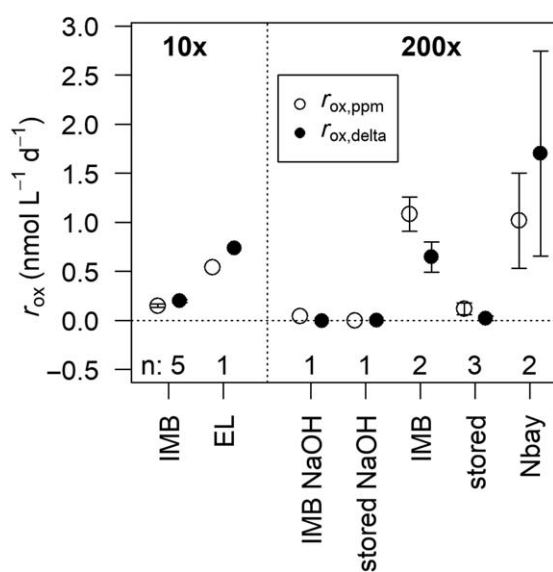


**Fig. 5.** CH<sub>4</sub> oxidation rates determined from CH<sub>4</sub> concentration ( $r_{ox,ppm}$ ) and isotope ratio ( $r_{ox,delta}$ ) at different spike concentrations (10×, 200×). Sampling sites are: EL, Utqiagvik Elson Lagoon; IMB, Utqiagvik ice mass balance buoy; IMB NaOH, Utqiagvik IMB with NaOH; Nbay, Narragansett Bay; stored, Utqiagvik IMB stored; stored NaOH, Utqiagvik IMB stored with NaOH. Error bars are standard deviations and  $n$  denotes the number of replicate incubations.

### Comparison with crimp top bottles

To compare the use of multi-layer foil incubators with other frequently used incubation vessels, we set up two incubation experiments with Utqiagvik IMB water in 145 mL crimp top bottles. For those a set of six replicate bottles were spiked with final concentrations of 50 nmol L<sup>-1</sup> (3×) and 400 nmol L<sup>-1</sup> (20×) (full details in Supporting Information Material). The bottles were successively fixed by the addition of sodium hydroxide and p(CH<sub>4</sub>) and  $\delta^{13}\text{CH}_4$  determined in duplicate from each bottle after completing the experiment. Oxidation rate constants in this first test were higher in the crimp bottles than in bags with similar methane concentration (Table 4; Fig. 4e–h). However, the spiked concentrations did not match exactly and thus preclude a direct comparison.

### Methane oxidation rates ( $r_{ox}$ )

The first order oxidation rate constants ( $k_{ox,ppm}$  and  $k_{ox,delta}$  (1.025)) and in situ methane concentrations, were used to calculate the in situ oxidation capability of the microbial communities in seawater from the Beaufort Sea and EL close to Point Barrow, Alaska, as well as in Narragansett Bay as described in Eq. 7. The 10× treatments showed oxidation at rates of 0.15 nmol L<sup>-1</sup> d<sup>-1</sup> and 0.20 nmol L<sup>-1</sup> d<sup>-1</sup> for  $r_{ox,ppm}$  and  $r_{ox,delta}$ , respectively (Fig. 5, Supporting Information Table 2). After a lag phase of 6 d, the 200× treatments show a fast decrease of c(CH<sub>4</sub>), with an oxidation rate of 1.08 nmol L<sup>-1</sup> d<sup>-1</sup> (Figs. 3a–d, 5). At the same time, CH<sub>4</sub> became enriched in <sup>13</sup>CH<sub>4</sub> and final  $\delta^{13}\text{CH}_4$  values were found to be positive. Note that our

calibration range for  $\delta^{13}\text{CH}_4$  ranged from  $-66.5\text{‰}$  to  $-23.0\text{‰}$  only, and the absolute value for the positive  $\delta^{13}\text{CH}_4$  is not well constrained. A far lower rate was observed for the same but stored water incubations (200× IMB stored) with rates of only 0.12 nmol L<sup>-1</sup> d<sup>-1</sup>. We assume that the microbial community changed during the storage time leading to a loss of methane oxidizing bacterial groups.

Microbial communities in the Utqiagvik EL 10× treatments showed oxidation rates of 0.54 nmol L<sup>-1</sup> d<sup>-1</sup> for  $r_{ox,ppm}$  and 0.73 nmol L<sup>-1</sup> d<sup>-1</sup> for  $r_{ox,delta}$  (Fig. 5). Narragansett Bay 200× incubations resulted in oxidation rates of 1.02 and 1.70 for  $r_{ox,ppm}$  and  $r_{ox,delta}$ , respectively.

All oxidation rates determined for the 10× and 200× treatments fall into the middle range of oxidation rates published for Arctic and Subarctic environments (Mau et al. 2013; Gentz et al. 2014; Damm et al. 2015; Steinle et al. 2015; Mau et al. 2017) or marine sites with extraordinarily high oxidation rates at oil spills or gas flares (Valentine et al. 2010; Steinle et al. 2016). Those studies mostly employed radioisotope labeled methane with short incubation times of hours up to 3 d. It has to be noted that the long incubation times in our study might have led to artefacts like changes in the microbial community, biofilm formation, or depletion of nutrients and thus should not be regarded as true in situ rates.

### Oxidative potential of bacterial communities

The lag phase—that was observed in the higher concentration incubation treatments—followed by a strong decrease of methane, indicates a shift of the bacterial community toward methane oxidizers or enhanced methane metabolism in the existing community. Changes in microbial communities toward increased fractions of hydrocarbon degraders or methane oxidizers have been observed for samples from the Deep-water Horizon oil spill and a gas blowout site in the North Sea (Valentine et al. 2010; Steinle et al. 2016). These studies report oxidation rates of 820 nmol L<sup>-1</sup> d<sup>-1</sup> and 498 nmol L<sup>-1</sup> d<sup>-1</sup>, respectively. The change in oxidation rate during our long duration incubations indicates that these experiments with amended methane may rather reflect the latent oxidative potential of the microbial community than the in situ oxidation rates. We can interpret these rates as an oxidative capacity of the microbial community when exposed to a methane hotspot, such as seep, vent, or other thermodynamically unstable geologic structure containing methane. Assuming successful adaptation of the methanotrophic community to the elevated methane concentration, we can calculate a potential oxidation rate ( $r_{ox,pot}$ ) from the first order rate constant  $k_{ox,ppm}$  and the methane concentration dissolved in the water  $c(\text{CH}_4)_w$  during the incubation experiments as  $r_{ox,pot} = k_{ox,ppm} \times c(\text{CH}_4)_w$ . Potential oxidation rates determined from water sampled at Utqiagvik IMB were  $r_{ox,pot} = 1.13$  nmol L<sup>-1</sup> d<sup>-1</sup> for the 10× treatment and 271 nmol L<sup>-1</sup> d<sup>-1</sup> for the 200× treatment (Supporting Information Table 3).

## Discussion

The ISMOFI method that we have evaluated here has three principal advantages. First, the foil laminate gas-tight bags could be an attractive alternative to incubations carried out in rigid gas tight containers. Because the bag is collapsible, it can be sampled repeatedly without adversely affecting the pressure (and thus the solubility equilibrium) in the incubator. With a similar rationale Chan et al. (2016), use 15 L custom made collapsible bags in a mesocosm study. The commercially available multilayer foil bag used in our study can store 1–10 L of air or water. These volumes lie in between the volumes of frequently used crimp top glass bottles (25–250 mL) (Scranton et al. 1993; Jakobs et al. 2013; Steinle et al. 2015, 2016), and the mesocosm bags described above. The respective volumes of water and headspace can be configured as part of the incubation design; larger headspace permits more gas removal for sampling, while larger water volume favors a larger number of methane oxidizers and thus more methane oxidation. This allows for performing studies which require a large sample volume or repeated sampling over a long incubation time and the possibility of multi-stage experiments in one incubator, while still being transportable. On the other hand, the gas permeability of the bags defines a lower limit of the detection range of  $0.001\text{--}0.005\text{ d}^{-1}$  for  $k_{\text{ox}}$ .

Next, the Picarro G2201-*i* can be an attractive analytical tool. It is compact and relatively easy to ship and operate in a variety of environments. However, the G2201-*i* with SSIM does require a compressed gas bottle of hydrocarbon free air, and 300 W of reliable A/C power. Similar to an isotope ratio mass spectrometer, the G2201-*i* permits quantitation of the stable isotopes of carbon, but is slightly less precise by approximately a factor of 2 (Damm et al. 2010). Whereas the manufacturer advises against determining concentrations using the SSIM, we observed good reproducibility ( $< 2\%$ ) in concentration measurement between replicate samples with the ISMOFI experimental configuration down to mixing ratios of 0.5 ppm (Table 3). To minimize the variability introduced by varying pressure during sample dilution in the SSIM, we accounted for the atmospheric and internal SSIM pressure (Eq. 1) using the instruments SSIM pressure readout. The latter additionally provides a good control of leak tightness of the SSIM, when monitoring the minimal pressure (approximately 2.5 Torr) during the evacuation of the SSIM dilution chamber. The measurement of stable isotope ratios is not sensitive to small dilution effects and is thus not affected by changes in the pressure in the SSIM. However, isotope ratios measured from samples with methane mixing ratio less than 1.8 ppm must be corrected to remove instrument bias. After correction, the precision of the low concentration samples is  $1.8\%$  compared to a precision of  $0.62\%$  of samples that have methane mixing ratios higher than 1.8 ppm (Fig. 1c).

In either case, stable isotopes provide an independent constraint on the methane oxidation. The ISMOFI method avoids using radioisotopes, which can be difficult to ship to remote locations, however, the method cannot resolve the exceedingly low oxidation rates that have been observed using radioisotope tracers (Mau et al. 2013; Steinle et al. 2015). The methane spike concentrations ( $50\text{--}120\text{ nmol L}^{-1}$ ) and incubation times ( $\geq 5\text{ d}$ ) used in this study are higher than for the sensitive  $^3\text{H-CH}_4$  method (Bussmann et al. 2015), and thus deviate further from in situ conditions. Yet, they are an order of magnitude lower than previously reported for applications of stable isotope additions (Chan et al. 2016; Leonte et al. 2017). To resolve oxidation, ISMOFI requires a certain minimum concentration of dissolved methane as start condition, which has to be supplied as stable isotope spike if in situ concentrations are low. The sensitivity study for example indicates that a start concentration of  $20\text{ nmol L}^{-1}$  can resolve an oxidation rate  $k_{\text{ox,delta}}$  of  $0.01\text{ d}^{-1}$  within 4 d.

The accuracy of  $k_{\text{ox,delta}}$  is dependent on the isotopic fractionation factor  $\alpha_{\text{ox}}$  for oxidation (Eq. 10). Better knowledge on fractionation factors in marine and polar systems and the environmental constraints that influence fractionation would help to improve the accuracy of this method (Fig. 4). The concentration and isotope data collected with our proposed experimental setup could be used to calculate  $\alpha_{\text{ox}}$  with Eq. 8. However, this leads to a dependence of  $k_{\text{ox,delta}}$  from  $c(\text{CH}_4)$  and would thus prohibit comparing  $k_{\text{ox,ppm}}$  and  $k_{\text{ox,delta}}$  as independent constraints. While agreeing within 20% for small changes in isotope ratio ( $10\times\text{IMB}$ , increase of  $10\%$ ),  $k_{\text{ox,ppm}}$  and  $k_{\text{ox,delta}}$  diverged for larger changes in isotope ratios ( $200\times\text{IMB}$  and Nbay, increase of  $90\%$ ). Possible effects like a nonlinearity in the range of high  $\delta^{13}\text{CH}_4$  might add to the difference between  $k_{\text{ox,ppm}}$  and  $k_{\text{ox,delta}}$  in these cases. Adding calibrations in the range of high  $\delta^{13}\text{CH}_4$  values (up to  $+67\%$ ) might straighten out some of the discrepancy.

The ISMOFI method further offers the potential to distinguish between multiple carbon pools if isotope labeling on different substrates is used. Insight on other carbon cycle related processes like  $\text{CH}_4$  production or respiration could be gained by including carbon dioxide concentrations and stable isotope ratios in the analysis. Both can be determined with the Picarro G2201-*i* simultaneously to methane concentration and isotope ratios.

## Comments and recommendations

The use of ISMOFI was shown to successfully resolve methane oxidation rates from seawater samples in amended oxidation experiments. The method can easily be adapted to other water samples, e.g., from freshwater environments and is particularly recommended at higher methane concentrations like found for example in lakes or glacier runoff (Dieser et al. 2014; Ricão Canelhas et al. 2016).

Based on our diffusion test and a first comparison with crimp top bottles, we evaluate the bags as reliable incubation vessels for analysis of methane oxidation in a headspace approach. The inner layer of the multilayer foil bags is polyethylene. According to the manufacturer's information, background levels of volatile organic carbon compounds might be present. An acid-wash as proposed by (Chan et al. 2016), would reduce possible contaminants leaching from the bags and is recommended in combination with a sterilization procedure. Incubation with 70% ethanol and complete removal of ethanol residues by flushing with sterile air was used in this study.

### Appendix A: Correction for removed sample volume

At each sampling time ( $t=i$ ) the removed sample ( $n(\text{CH}_4)_{\text{sampled}}$ ) and the methane oxidized by bacteria ( $n(\text{CH}_4)_{\text{ox}}$ ) are accounted for as follows:

$$n(\text{CH}_4)_{\text{total}, t_i} = n(\text{CH}_4)_{\text{total}, t_{i-1}} - \left( n(\text{CH}_4)_{\text{ox}, t_{i-1} \text{ to } t_i} + n(\text{CH}_4)_{\text{sampled}, t_{i-1} \text{ to } t_i} \right) \quad (12)$$

The amount of  $\text{CH}_4$  removed from the headspace during sampling ( $n(\text{CH}_4)_{\text{sampled}, t_i}$ ) was calculated as the mean of the mass of  $\text{CH}_4$  of all replicates at  $t=i$  ( $n(\text{CH}_4)_{\text{hs}, t_i}$ ) times the fraction of the total volume of replicate samplings at  $t=i$  ( $V(\text{CH}_4)_{\text{sampled}, t_i}$ ) of the headspace volume at the start of sampling  $t=i$  ( $V(\text{CH}_4)_{\text{hs}, t_i}$ ).

$$n(\text{CH}_4)_{\text{sampled}, t_i} = n(\text{CH}_4)_{\text{hs}, t_i} \times \frac{V(\text{CH}_4)_{\text{sampled}, t_i}}{V(\text{CH}_4)_{\text{hs}, t_i}} \quad (13)$$

For example, if three sampling replicates of 10 mL were removed by syringe from a bag with 150 mL headspace, the ratio  $\frac{V(\text{CH}_4)_{\text{sampled}, t_i}}{V(\text{CH}_4)_{\text{hs}, t_i}}$  would be  $\frac{30}{150}$ .

### Appendix B: Definition of the isotopic fractionation factor

In a closed system, it is valid to apply a model after Rayleigh (1896). For the oxidation of methane and the isotope ratios in the residual pool

$$\frac{d^{13}\text{CH}_4}{d^{12}\text{CH}_4} = \frac{k_{13}}{k_{12}} \times \frac{^{13}\text{CH}_4}{^{12}\text{CH}_4} \quad (14)$$

with  $^{13}\text{CH}_4/^{12}\text{CH}_4$  as the ratio of the quantities of isotopes in the residual methane,  $d^{13}\text{CH}_4/d^{12}\text{CH}_4$  the ratio of the isotopes of the product in an infinitesimal small amount of time (Mahieu et al. 2006), and  $k_{12}$  and  $k_{13}$  the kinetic constants for reactions of the heavier and lighter isotope  $\text{CH}_4$ . The ratio between the kinetic constants is the isotopic fractionation factor  $\alpha$ . Here, we use the definition of  $\alpha_{\text{ox}} = k_{12}/k_{13}$  (Mahieu et al. 2006). It should be noted that several other studies (Mariotti et al. 1981; Whiticar 1999) use the reciprocal value ( $\alpha_{\text{rec}} = k_{13}/k_{12}$ ).

### References

- Abril, G., M.-V. Commarieu, and F. Guérin. 2007. Enhanced methane oxidation in an estuarine turbidity maximum. *Limnol. Oceanogr.* **52**: 470–475. doi:10.4319/lo.2007.52.1.0470
- Andrade, J. M., and M. G. Estévez-Pérez. 2014. Statistical comparison of the slopes of two regression lines: A tutorial. *Anal. Chim. Acta* **838**: 1–12. doi:10.1016/j.aca.2014.04.057
- Barnes, R. O., and E. D. Goldberg. 1976. Methane production and consumption in anoxic marine sediments. *Geology* **4**: 297. doi:10.1130/0091-7613(1976)4 <297:MPACIA>2.0.CO;2
- Bastviken, D., J. Ejlertsson, and L. Tranvik. 2002. Measurement of methane oxidation in lakes: A comparison of methods. *Environ. Sci. Technol.* **36**: 3354–3361. doi:10.1021/es010311p
- Boetius, A., and F. Wenzhöfer. 2013. Seafloor oxygen consumption fuelled by methane from cold seeps. *Nat. Geosci.* **6**: 725–734. doi:10.1038/ngeo1926
- Bussmann, I., A. Matousu, R. Osudar, and S. Mau. 2015. Assessment of the radio  $^3\text{H}\text{-CH}_4$  tracer technique to measure aerobic methane oxidation in the water column: The  $^3\text{H}\text{-CH}_4$  tracer technique to measure aerobic methane oxidation. *Limnol. Oceanogr.: Methods* **13**: 312–327. doi:10.1002/lom3.10027
- Chan, E. W., J. D. Kessler, A. M. Shiller, D. Joung, and F. Colombo. 2016. Aqueous mesocosm techniques enabling the real-time measurement of the chemical and isotopic kinetics of dissolved methane and carbon dioxide. *Environ. Sci. Technol.* **50**: 3039–3046. doi:10.1021/acs.est.5b04304
- Cowen, J. P., X. Wen, and B. N. Popp. 2002. Methane in aging hydrothermal plumes. *Geochim. Cosmochim. Acta* **66**: 3563–3571. doi:10.1016/S0016-7037(02)00975-4
- Crespo-Medina, M., and others. 2014. The rise and fall of methanotrophy following a deepwater oil-well blowout. *Nat. Geosci.* **7**: 423–427. doi:10.1038/ngeo2156
- Damm, E., U. Schauer, B. Rudels, and C. Haas. 2007. Excess of bottom-released methane in an Arctic shelf sea polynya in winter. *Cont. Shelf Res.* **27**: 1692–1701. doi:10.1016/j.csr.2007.02.003
- Damm, E., R. P. Kiene, J. Schwarz, E. Falck, and G. Dieckmann. 2008. Methane cycling in Arctic shelf water and its relationship with phytoplankton biomass and DMSP. *Mar. Chem.* **109**: 45–59. doi:10.1016/j.marchem.2007.12.003
- Damm, E., E. Helmke, S. Thoms, U. Schauer, E. Nöthig, K. Bakker, and R. P. Kiene. 2010. Methane production in aerobic oligotrophic surface water in the central Arctic Ocean. *Biogeosciences* **7**: 1099–1108. doi:10.5194/bg-7-1099-2010
- Damm, E., B. Rudels, U. Schauer, S. Mau, and G. Dieckmann. 2015. Methane excess in Arctic surface water- triggered by sea ice formation and melting. *Sci. Rep.* **5**: 16179. doi:10.1038/srep16179
- Dieser, M., and others. 2014. Molecular and biogeochemical evidence for methane cycling beneath the western margin

- of the Greenland Ice Sheet. *ISME J.* **8**: 2305–2316. doi:[10.1038/ismej.2014.59](https://doi.org/10.1038/ismej.2014.59)
- Fenwick, L., D. Capelle, E. Damm, S. Zimmermann, W. J. Williams, S. Vagle, and P. D. Tortell. 2017. Methane and nitrous oxide distributions across the North American Arctic Ocean during summer, 2015: CH<sub>4</sub> AND N<sub>2</sub>O distributions in Arctic Ocean. *J. Geophys. Res. Oceans* **122**: 390–412. doi:[10.1002/2016JC012493](https://doi.org/10.1002/2016JC012493)
- Formolo, M. 2010. The microbial production of methane and other volatile hydrocarbons, p. 113–126. *In* K. N. Timmis [ed.], *Handbook of hydrocarbon and lipid microbiology*. Springer.
- Fuex, A. N. 1980. Experimental evidence against an appreciable isotopic fractionation of methane during migration. *Phys. Chem. Earth* **12**: 725–732. doi:[10.1016/0079-1946\(79\)90153-8](https://doi.org/10.1016/0079-1946(79)90153-8)
- Garcia, H. E., and L. I. Gordon. 1992. Oxygen solubility in seawater: Better fitting equations. *Limnol. Oceanogr.* **37**: 1307–1312. doi:[10.4319/lo.1992.37.6.1307](https://doi.org/10.4319/lo.1992.37.6.1307)
- Gentz, T., E. Damm, J. Schneider von Deimling, S. Mau, D. F. McGinnis, and M. Schlüter. 2014. A water column study of methane around gas flares located at the West Spitsbergen continental margin. *Cont. Shelf Res.* **72**: 107–118. doi:[10.1016/j.csr.2013.07.013](https://doi.org/10.1016/j.csr.2013.07.013)
- Grant, N. J., and M. J. Whiticar. 2002. Stable carbon isotopic evidence for methane oxidation in plumes above Hydrate Ridge, Cascadia Oregon Margin. *Global Biogeochem. Cycles* **16**: 71-1-71-13. doi:[10.1029/2001GB001851](https://doi.org/10.1029/2001GB001851)
- Hanson, R. S., and T. E. Hanson. 1996. Methanotrophic bacteria. *Microbiol. Rev.* 439–471.
- IPCC. 2013. Carbon and other biogeochemical cycles. *In* T. F. Stocker, and others [eds.], *Climate change 2013: The physical science basis. Contribution of working group I to the fifth assessment report of the intergovernmental panel on climate change*. 465–570. Cambridge Univ. Press.
- Jakobs, G., G. Rehder, G. Jost, K. Kießlich, M. Labrenz, and O. Schmale. 2013. Comparative studies of pelagic microbial methane oxidation within the redox zones of the Gotland Deep and Landsort Deep (central Baltic Sea). *Biogeosciences* **10**: 7863–7875. doi:[10.5194/bg-10-7863-2013](https://doi.org/10.5194/bg-10-7863-2013)
- James, R. H., and others. 2016. Effects of climate change on methane emissions from seafloor sediments in the Arctic Ocean: A review. *Limnol. Oceanogr.* **61**: S283–S299. doi:[10.1002/lno.10307](https://doi.org/10.1002/lno.10307)
- Karl, D. M., L. Beversdorf, K. M. Björkman, M. J. Church, A. Martinez, and E. F. Delong. 2008. Aerobic production of methane in the sea. *Nat. Geosci.* **1**: 473–478. doi:[10.1038/ngeo234](https://doi.org/10.1038/ngeo234)
- Kessler, J. D., and others. 2011. A persistent oxygen anomaly reveals the fate of spilled methane in the deep Gulf of Mexico. *Science* **331**: 312–315. doi:[10.1126/science.1199697](https://doi.org/10.1126/science.1199697)
- Knittel, K., and A. Boetius. 2009. Anaerobic oxidation of methane: Progress with an unknown process. *Annu. Rev. Microbiol.* **63**: 311–334. doi:[10.1146/annurev.micro.61.080706.093130](https://doi.org/10.1146/annurev.micro.61.080706.093130)
- Kvenvolden, K. A., M. D. Lilley, T. D. Lorenson, P. W. Barnes, and E. McLaughlin. 1993. The Beaufort Sea continental shelf as a seasonal source of atmospheric methane. *Geophys. Res. Lett.* **20**: 2459–2462. doi:[10.1029/93GL02727](https://doi.org/10.1029/93GL02727)
- Kvenvolden, K. A., and B. W. Rogers. 2005. Gaia's breath—global methane exhalations. *Mar. Pet. Geol.* **22**: 579–590. doi:[10.1016/j.marpetgeo.2004.08.004](https://doi.org/10.1016/j.marpetgeo.2004.08.004)
- Lecher, A. L., J. Kessler, K. Sparrow, F. Garcia-Tigreros Kodovska, N. Dimova, J. Murray, S. Tulaczyk, and A. Paytan. 2016. Methane transport through submarine groundwater discharge to the North Pacific and Arctic Ocean at two Alaskan sites. *Limnol. Oceanogr.* **61**: S344–S355. doi:[10.1002/lno.10118](https://doi.org/10.1002/lno.10118)
- Leonte, M., J. D. Kessler, M. Y. Kellermann, E. C. Arrington, D. L. Valentine, and S. P. Sylva. 2017. Rapid rates of aerobic methane oxidation at the feather edge of gas hydrate stability in the waters of Hudson Canyon, US Atlantic Margin. *Geochim. Cosmochim. Acta* **204**: 375–387. doi:[10.1016/j.gca.2017.01.009](https://doi.org/10.1016/j.gca.2017.01.009)
- Loose, B., and others. 2011. Gas diffusion through columnar laboratory sea ice: Implications for mixed-layer ventilation of CO<sub>2</sub> in the seasonal ice zone. *Tellus B* **63**: 23–39. doi:[10.1111/j.1600-0889.2010.00506.x](https://doi.org/10.1111/j.1600-0889.2010.00506.x)
- Magen, C., L. L. Lapham, J. W. Pohlman, K. Marshall, S. Bosman, M. Casso, and J. P. Chanton. 2014. A simple headspace equilibration method for measuring dissolved methane. *Limnol. Oceanogr.: Methods* **12**: 637–650. doi:[10.4319/lom.2014.12.637](https://doi.org/10.4319/lom.2014.12.637)
- Mahieu, K., A. D. Visscher, P. A. Vanrolleghem, and O. V. Cleemput. 2006. Carbon and hydrogen isotope fractionation by microbial methane oxidation: Improved determination. *Waste Manag.* **26**: 389–398. doi:[10.1016/j.wasman.2005.11.006](https://doi.org/10.1016/j.wasman.2005.11.006)
- Mariotti, A., J. C. Germon, P. Hubert, P. Kaiser, R. Letolle, A. Tardieux, and P. Tardieux. 1981. Experimental determination of nitrogen kinetic isotope fractionation: Some principles; illustration for the denitrification and nitrification processes. *Plant Soil* **62**: 413–430. doi:[10.1007/BF02374138](https://doi.org/10.1007/BF02374138)
- Mau, S., M. B. Heintz, and D. L. Valentine. 2012. Quantification of CH<sub>4</sub> loss and transport in dissolved plumes of the Santa Barbara Channel, California. *Cont. Shelf Res.* **32**: 110–120. doi:[10.1016/j.csr.2011.10.016](https://doi.org/10.1016/j.csr.2011.10.016)
- Mau, S., J. Blees, E. Helmke, H. Niemann, and E. Damm. 2013. Vertical distribution of methane oxidation and methanotrophic response to elevated methane concentrations in stratified waters of the Arctic fjord Storfjorden (Svalbard, Norway). *Biogeosciences* **10**: 6267–6278. doi:[10.5194/bg-10-6267-2013](https://doi.org/10.5194/bg-10-6267-2013)
- Mau, S., and others. 2017. Widespread methane seepage along the continental margin off Svalbard - from Bjørnøya to Kongsfjorden. *Sci. Rep.* **7**: 42997. doi:[10.1038/srep42997](https://doi.org/10.1038/srep42997)
- McKinney, C. R., J. M. McCrea, S. Epstein, H. A. Allen, and H. C. Urey. 1950. Improvements in mass spectrometers for the measurement of small differences in isotope abundance ratios. *Rev. Sci. Instrum.* **21**: 724. doi:[10.1063/1.1745698](https://doi.org/10.1063/1.1745698)

- Murrell, J. C. 2010. The aerobic methane oxidizing bacteria (Methanotrophs), p. 1953–1966. *In* K. N. Timmis [ed.], *Handbook of hydrocarbon and lipid microbiology*. Springer.
- Pack, M. A., M. B. Heintz, W. S. Reeburgh, S. E. Trumbore, D. L. Valentine, X. Xu, and E. R. M. Druffel. 2015. Methane oxidation in the eastern tropical North Pacific Ocean water column. *J. Geophys. Res. Biogeosci.* **120**: 1078–1092. doi:10.1002/2014JG002900
- Rayleigh, L.S.R.S. 1896. L. Theoretical considerations respecting the separation of gases by diffusion and similar processes. *Philos. Mag. Ser. 5.* **42**: 493–498. doi:10.1080/14786449608620944
- Reeburgh, W. S. 1976. Methane consumption in Cariaco Trench waters and sediments. *Earth Planet. Sci. Lett.* **28**: 337–344. doi:10.1016/0012-821X(76)90195-3
- Reeburgh, W. S. 2007. Oceanic methane biogeochemistry. *Chem. Rev.* **107**: 486–513. doi:10.1021/cr050362v
- Reeburgh, W. S., B. B. Ward, S. C. Whalen, K. A. Sandbeck, K. A. Kilpatrick, and L. J. Kerkhof. 1991. Black Sea methane geochemistry. *Deep-Sea Res. Part A Oceanogr. Res. Pap.* **38**: S1189–S1210. doi:10.1016/S0198-0149(10)80030-5
- Ricão Canelhas, M., B. A. Denfeld, G. A. Weyhenmeyer, D. Bastviken, and S. Bertilsson. 2016. Methane oxidation at the water-ice interface of an ice-covered lake: Methane oxidation at the water-ice interface. *Limnol. Oceanogr.* **61**: S78–S90. doi:10.1002/lno.10288
- Sansone, F. J., B. N. Popp, A. Gasc, A. W. Graham, and T. M. Rust. 2001. Highly elevated methane in the eastern tropical North Pacific and associated isotopically enriched fluxes to the atmosphere. *Geophys. Res. Lett.* **28**: 4567–4570. doi:10.1029/2001GL013460
- Saunois, M., and others. 2016. The global methane budget 2000–2012. *Earth Syst. Sci. Data* **8**: 697–751. doi:10.5194/essd-8-697-2016
- Scranton, M. I., and P. G. Brewer. 1978. Consumption of dissolved methane in the deep ocean. *Limnol. Oceanogr.* **23**: 1207–1213. doi:10.4319/lno.1978.23.6.1207
- Scranton, M. I., P. Crill, M. A. de Angelis, P. L. Donaghay, and J. M. Sieburth. 1993. The importance of episodic events in controlling the flux of methane from an anoxic basin. *Global Biogeochem. Cycles* **7**: 491–507. doi:10.1029/93GB00869
- Semrau, J. D., A. A. DiSpirito, and S. Yoon. 2010. Methanotrophs and copper. *FEMS Microbiol. Rev.* **34**: 496–531. doi:10.1111/j.1574-6976.2010.00212.x
- Shakhova, N., I. Semiletov, A. Salyuk, V. Yusupov, D. Kosmach, and Ö. Gustafsson. 2010. Extensive methane venting to the atmosphere from sediments of the East Siberian Arctic shelf. *Science* **327**: 1246–1250. doi:10.1126/science.1182221
- Steinle, L., and others. 2015. Water column methanotrophy controlled by a rapid oceanographic switch. *Nat. Geosci.* **8**: 378–382. doi:10.1038/ngeo2420
- Steinle, L., and others. 2016. Linked sediment and water-column methanotrophy at a man-made gas blowout in the North Sea: Implications for methane budgeting in seasonally stratified shallow seas: Linked sediment and water methanotrophy. *Limnol. Oceanogr.* **61**: S367–S386. doi:10.1002/lno.10388
- Valentine, D. L., D. C. Blanton, W. S. Reeburgh, and M. Kastner. 2001. Water column methane oxidation adjacent to an area of active hydrate dissociation, Eel river Basin. *Geochim. Cosmochim. Acta* **65**: 2633–2640. doi:10.1016/S0016-7037(01)00625-1
- Valentine, D. L., and others. 2010. Propane respiration jump-starts microbial response to a deep oil spill. *Science* **330**: 208–211. doi:10.1126/science.1196830
- Welch, B. L. 1938. The significance of the difference between two means when the population variances are unequal. *Biometrika* **29**: 350–362. doi:10.2307/2332010
- Whiticar, M. J. 1999. Carbon and hydrogen isotope systematics of bacterial formation and oxidation of methane. *Chem. Geol.* **161**: 291–314. doi:10.1016/S0009-2541(99)00092-3
- Yamamoto, S., J. B. Alcauskas, and T. E. Crozier. 1976. Solubility of methane in distilled water and seawater. *J. Chem. Eng. Data* **21**: 78–80. doi:10.1021/je60068a029
- Zhou, J., J.-L. Tison, G. Carnat, N.-X. Geilfus, and B. Delille. 2014. Physical controls on the storage of methane in landfast sea ice. *Cryosphere* **8**: 1019–1029. doi:10.5194/tc-8-1019-2014

#### Acknowledgment

We thank Clarisse Sullivan for help with preparations for fieldwork and John B. Kirkpatrick for support during fieldwork. We appreciate the comments of three anonymous reviewers that improved the manuscript. This work was supported the American Chemical Society, Petroleum Research Fund (PRF# 54473-DNI2).

#### Conflict of Interest

None declared.

Submitted 16 January 2017

Revised 26 April 2017; 15 June 2017

Accepted 26 June 2017

Associate editor: Krista Longnecker